




Article

Effects of Different Fields of View and Rotation Angles on Radiation Doses to Highly Radiosensitive Organs in Children Using Dental Cone Beam Computed Tomography

Misaki Ito ^{1,2}, Ikuho Kojima ^{3,4} , Masahiro Iikubo ^{3,4} , Shu Onodera ¹, Masahiro Sai ¹, Masaki Fujisawa ², Toshiki Kato ², Masaaki Nakamura ², Masayuki Zuguchi ² and Koichi Chida ^{2,5,*} 

¹ Radiological Technology, Tohoku University Hospital, 1-1 Seiryomachi, Aoba-ku, Sendai 980-8574, Japan; misaki.sinoda.t5@dc.tohoku.ac.jp (M.I.); shu.onodera.e2@tohoku.ac.jp (S.O.); masahiro.sai.d8@tohoku.ac.jp (M.S.)

² Department of Radiological Technology, Tohoku University Graduate School of Medicine, 2-1 Seiryomachi, Aoba-ku, Sendai 980-8575, Japan; masaki.fujisawa.q1@dc.tohoku.ac.jp (M.F.); toshiki.kato.r8@dc.tohoku.ac.jp (T.K.); nakamura.masaaki@nifty.com (M.N.); qqrm6wq9k@arrow.ocn.ne.jp (M.Z.)

³ Division of Oral and Maxillofacial Radiology, Tohoku University Hospital, 1-1 Seiryomachi, Aoba-ku, Sendai 980-8574, Japan; ikuhokojima@tohoku.ac.jp (I.K.); machapy@tohoku.ac.jp (M.I.)

⁴ Division of Dental Informatics and Radiology, Tohoku University Graduate School of Dentistry, 4-1 Seiryomachi, Aoba-ku, Sendai 980-8575, Japan

⁵ Division of Disaster Medical Science, International Research Institute of Disaster Science, Tohoku University, 468-1 Aoba, Aramaki, Aoba-ku, Sendai 980-8572, Japan

* Correspondence: chida@med.tohoku.ac.jp

Featured Application: Importance of the evaluation of radiation doses to highly radiosensitive organs in children using dental cone beam computed tomography, given that children are highly sensitive to radiation.



Citation: Ito, M.; Kojima, I.; Iikubo, M.; Onodera, S.; Sai, M.; Fujisawa, M.; Kato, T.; Nakamura, M.; Zuguchi, M.; Chida, K. Effects of Different Fields of View and Rotation Angles on Radiation Doses to Highly Radiosensitive Organs in Children Using Dental Cone Beam Computed Tomography. *Appl. Sci.* **2024**, *14*, 9154. <https://doi.org/10.3390/app14199154>

Academic Editor: Miguel Alcaraz

Received: 1 September 2024

Revised: 27 September 2024

Accepted: 4 October 2024

Published: 9 October 2024



Copyright: © 2024 by the authors. Licensee MDPI, Basel, Switzerland. This article is an open access article distributed under the terms and conditions of the Creative Commons Attribution (CC BY) license (<https://creativecommons.org/licenses/by/4.0/>).

Abstract: Dental cone beam computed tomography (CBCT) is a diverse 3D X-ray imaging technique that has enabled clear visualization of the teeth and surrounding structures. The most common diagnostic purpose of dental CBCT examination in children is ectopic eruption and impacted teeth, and a small field of view (FOV) is often used. Since it is difficult for children to control their body movements, reducing the rotation angle is effective. However, no studies have examined the effects of different rotation angles on radiation doses to highly radiosensitive organs in children using small FOVs. The purpose of this study was to examine the effects of small FOVs (4 × 4 cm and 6 × 6 cm) and rotation angles (360° and 180°) on doses that highly sensitize organs in children using dental CBCT. The entrance surface doses to lenses, thyroid lobes, parotid glands, and sublingual glands of a pediatric whole-body phantom were measured. By reducing the FOV from 6 × 6 cm to 4 × 4 cm, the dose to the sublingual gland could be significantly decreased. Additionally, by reducing the rotation angle from 360° to 180°, the lens dose can be decreased significantly. As the rate of dose reduction varies among organs, it is important to consider the relative positions of different organs with respect to the FOV and the trajectory of the X-ray tube.

Keywords: dental; cone beam computed tomography (CBCT); child; radiation dosimetry; field of view (FOV); rotation angles; eye lens; radiation dose; thyroid lobe dose

1. Introduction

Radiographic examinations are of great benefit to patients by visualizing conditions inside the body, which helps in the diagnosis of diseases and treatment strategies. However, there is a risk of radiation exposure due to the use of radiation [1–4]. In Publication 118, the International Commission on Radiological Protection (ICRP) published a review of recent

epidemiological evidence and concluded that the threshold doses for very late effects, such as cataracts, are lower than previously thought [5]. In 2011, ICRP revised its eye dose threshold for cataract induction downwards from 8 Gy to 0.5 Gy [5,6]. Therefore, evaluation of lens exposure in particular is becoming more important [7–14]. Since teeth and periodontal tissues that are the focus of dental radiography are close to the lens, it is critical to measure the exposure dose to the lens in dental radiography as well.

Popular dental X-ray imaging procedures include intraoral radiography, panoramic radiography, and cone beam computed tomography (CBCT). The intraoral radiography provides high spatial resolution imaging of teeth and periodontal tissue and has often been used to detect periodontal disease and cavities [15–19]. Panoramic radiography, a single curved tomographic image, provides a wide range of information about the dentition, alveolar bone, and surrounding structures of both jaws. CBCT is a diverse 3D X-ray imaging technique that has enabled the clear visualization of the teeth and surrounding structures. It gives a lower radiation exposure to patients than multi-slice CT, but the exposure is more than that of intraoral and panoramic radiography [20–27].

Childhood is the period when baby teeth become permanent; the development of the oral cavity is remarkable, and the dental structure is complex. Therefore, dental CBCT, which can capture the anatomical structure and positional relationship of teeth and periodontal tissues in three dimensions, is sometimes used for pediatric dental diagnosis and has been applied to very young patients. In the study conducted by Hidalgo-Rivas et al. [28] in the UK, the youngest patients with CBCT requests were 5 years old. Ebru et al. [29] reported that the youngest patient was aged 4 years.

Children are more sensitive to radiation than adults; therefore, it is necessary to reduce the exposure dose as much as possible [30–36]. Theodorakou et al. [37] reported a lifetime mortality risk imputed fraction of 0.00174% for 10 year olds using CBCT examinations, which was considerably higher than that for adults receiving the same dose (0.00075%). According to Pauwels et al. [38], the lifetime attributable cancer risk, expressed as the probability of developing radiation-induced cancer, varied between 2.7 per million (age > 60 years) and 9.8 per million (age 8–11 years) with an average of 6.0 per million (age 8–83 years). It is important to assess and quantify radiation risks in children.

The purpose of CBCT in children is to diagnose ectopic eruptions, impacted teeth, traumatized teeth, and intraosseous cysts or tumors. Among these, the rates of ectopic eruption and impacted teeth are particularly high [25,28,39,40]. The number of ectopic eruptions and impacted teeth per pediatric patient is often a single tooth, and in most cases, a small field of view (FOV) is sufficient for the examination [41–43]. General guidelines recommend keeping the FOV as small as possible to include only the region of interest [44]. Several studies have measured radiation doses to highly radiosensitive organs using small FOVs (<40 cm²) in adults [45–47]. However, to the best of our knowledge, no studies have examined them in children. It is important to understand the FOVs and relative positions of radiation-sensitive organs, even in children, because of the differences in head and neck sizes between adults and children.

One method to reduce radiation dose is 180° rotation. As children are more likely to move during imaging than adults, the 180° rotation, shorter imaging time, is considered effective for children. However, Hajem et al. [48] reported that 360° rotation is used more often than 180° rotation in dental CBCT examinations of children.

The purpose of this study was to examine the effects of FOVs and rotation angles on radiation doses to highly radiosensitive organs in children using dental CBCT, and to clarify the usefulness of reducing the FOV and rotation angle in children.

2. Materials and Methods

This study was performed using a 3D Accuitomo F17 (Dental CBCT system, J. Morita, Kyoto, Japan) equipped with a flat-panel detector (FPD) of an indirect type made of cesium iodide (CsI). Dental CBCT examinations were performed by positioning a pediatric whole-body phantom (PBU-70; Kyoto Kagaku Co., Ltd., Kyoto, Japan) in the same position used

for the patient examinations. The experimental layout is shown in Figure 1. The phantom was modeled after a 5-year-old child who was 110 cm in height. The phantom consists of a synthetic skeleton with the synthetic lungs, liver, mediastinum, and kidneys embedded in a soft-tissue substitute.

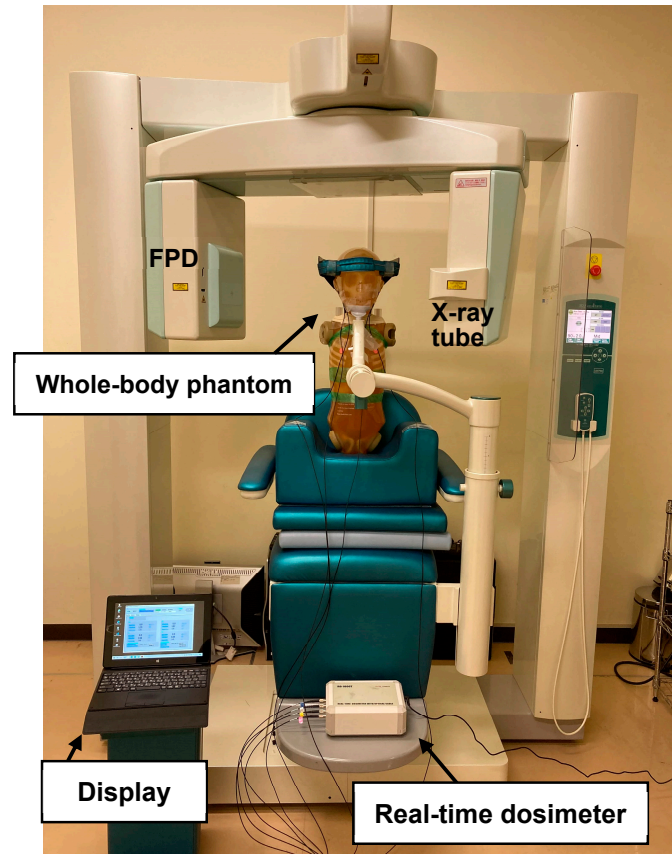


Figure 1. Experimental layout.

This equipment requires manual setting of the exposure factors. In our previous study [49], we determined the tube voltage characteristics of an FPD installed in a CBCT. Among the tube voltages examined, the X-ray photon detection rate for the FPD was the highest at 90 kV, and the radiation dose was the lowest. Therefore, a tube voltage of 90 kV was used at all time points. In addition, in our previous study [50], we examined the optimal protocols for diagnosing ectopic eruptions and impacted teeth in children using different tube currents, FOVs, and rotation angles while using a tube voltage of 90 kV. Based on radiation doses and physical and visual evaluations, the optimal protocols were determined to be 2 mA, 4×4 cm FOV, and 180° rotation. However, 1 mA was not suitable for diagnosis due to image noise and artifacts. Furthermore, tube currents of 2 and 3 mA were examined because tube currents greater than 3 mA could significantly exceed National Diagnostic Reference Levels (NDRLs) for the UK [51]. In this study, eight combinations of tube voltage (90 kV), tube current (2 and 3 mA), FOVs (4×4 cm and 6×6 cm), and rotation angles (360° and 180°) were used. Imaging conditions are presented in Table 1. Exposure time is 17.5 s for 360° rotation and 9.0 s for 180° rotation. A 180° rotation can be used to reduce the exposure doses, and the X-ray tube rotates around the posterior aspect of the phantom. X-ray irradiation image is shown in Figure 2.

Table 1. Imaging conditions.

| Parameter | Value |
|--------------------|--------------|
| Tube voltage (kV) | 90 |
| Tube current (mA) | 2, 3 |
| Field of view (cm) | 4 × 4, 6 × 6 |
| Rotation angle (°) | 360, 180 |

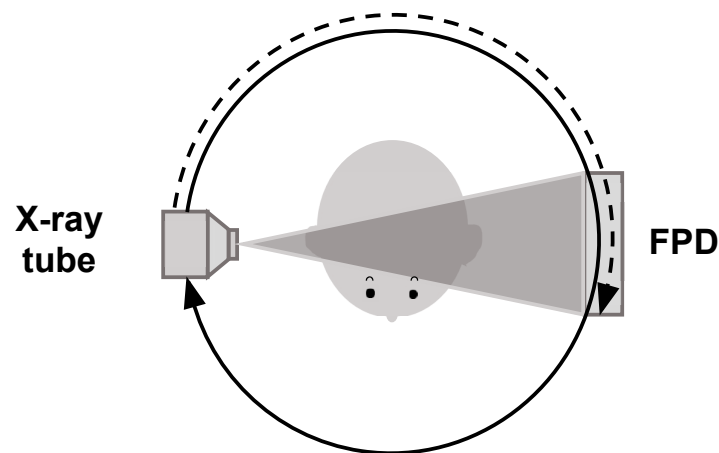


Figure 2. X-ray irradiation image. Solid line indicates 360° imaging: X-rays are radiated at 360° angle; dotted line indicates 180° imaging: X-rays are radiated at 180° + fan angle.

Generally, in dental CBCT, the center of FOV and the center of rotation are at the same position because the target tooth is placed at the center of rotation. The maxillary median and maxillary right canine were centered in the FOV on scout images because the maxillary incisors and canines are common sites for ectopic eruption and impacted teeth in children [25,52–60]. Nikhil et al. [61] reported that 90–98% of ectopic eruptions and impacted teeth occur in the maxilla, with a particular predilection for the premaxilla. The positions of the center of the FOVs on the scout images are shown in Figure 3. CBCT scans were performed thrice for each imaging condition and position.

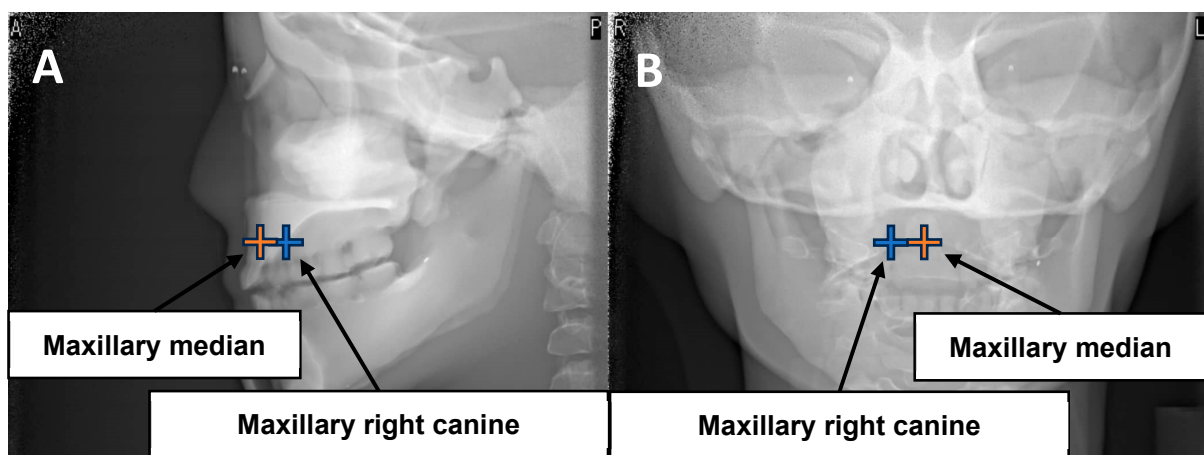


Figure 3. The positions of the center of the FOVs on the scout images: (A) anteroposterior scout and (B) lateral scout.

An optical cable-type real-time dosimeter (RTD) (RD-1000; Toreck Co., Ltd., Yokohama, Japan) was used to measure the entrance surface dose. This RTD consisted of photoluminescence sensors ($Y_2O_2S: Eu, Sm$), an optical fiber cable, a photodiode, and a digital display that included the power supply, and can measure using a maximum of four sensors

(ch.1, ch.2, ch.3, and ch.4) in one measurement. In previous studies, the RTD demonstrated good fundamental characteristics related to energy dependence, dose linearity, dose rate dependence, and angular dependence [62–64]. The entrance surface doses to the lenses, thyroid lobes, parotid glands, and sublingual glands were measured because these organs are radiosensitive in the head and neck region [65]. First, the sensors were placed at positions corresponding to the right and left lenses and thyroid lobes on the surface of the phantom (ch.1: right lens; ch.2: left lens; ch.3: right lobe of thyroid; and ch.4: left lobe of thyroid). Next, the sensors were placed at positions corresponding to the right and left parotid and sublingual glands on the surface of the phantom, as shown in Figure 4 (ch.1: right parotid gland; ch.2: left parotid gland; ch.3: right sublingual gland; and ch.4: left sublingual gland). Sensors of the dosimeter were attached to the surface of the phantom, because we did not have a child phantom in which dosimeters could be placed inside. Since the actual organs are distributed at a small distance from the body surface, for more accurate dosimetry, the sensors of the dosimeter must be embedded within the phantom.

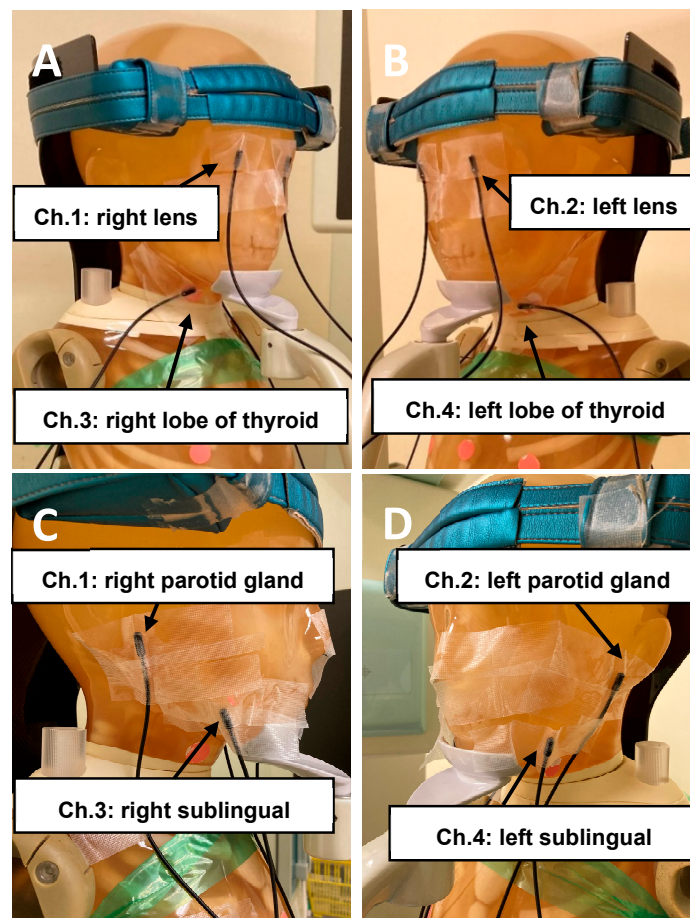


Figure 4. RTDs were placed on lens, thyroid, parotid gland, and sublingual gland surfaces of the phantom surfaces of the pediatric whole-body phantom. Position of the dosimeter for measuring (A) the right lens, right lobe of thyroid, (B) left lens, left lobe of thyroid, (C) right parotid, right sublingual, and (D) left parotid, and left sublingual.

Dose calibration of RTD was performed against an ionization chamber dosimeter (9015, Radcal Corporation, Monrovia, CA, USA) with a 6 cm³ thimble ionization chamber (10X5–6, Radcal Corporation) traceable to a national standard. The chamber dosimeter and RTD were placed freely in air adjacent to each other in the irradiated field at the same distance from the X-ray focus. The correction factor was determined using this calibration procedure.

Furthermore, the entrance surface dose was converted to the dose by each organ by multiplying the mass energy absorption coefficient ratio for each organ to air from Publication 44 of the International Commission on Radiation Units and Measurements (ICRU) (lens: 0.94; thyroid: 1.15). For other organs (i.e., the parotid and sublingual gland), no specific coefficients are available in ICRU Publication 44 [66]. Considering that the correction factors for most soft tissue organs were close to 1, no correction was applied to these two organs. However, in this study, the dosimeters were attached to the surface of the phantom, so the organ-absorbed dose could not be calculated accurately. Therefore, the entrance surface dose was approximated to the organ-absorbed dose by multiplying the entrance surface dose by the coefficient ratio.

3. Results

Table 2 shows the results of radiation doses to highly radiosensitive organs measured with the maxillary median placed at the center of rotation. Table 3 shows the results of radiation doses to highly radiosensitive organs measured with the maxillary right canine tooth placed at the center of rotation. For both the maxillary median and right canine, the parotid gland doses were significantly higher than the other organ doses examined in the 4×4 cm FOV. Compared with the 4×4 cm FOV, the sublingual gland doses increased significantly at the 6×6 cm FOV.

Compared with the maxillary median, the dose to the right sublingual gland was slightly higher in the 6×6 cm FOV with the maxillary right canine tooth placed at the center of rotation.

When the FOV was reduced from 6×6 cm to 4×4 cm, the reduction rates of the doses to the lenses, thyroid lobes, parotid glands, and sublingual glands were approximately 38.2–62.5%, 58.8–71.2%, 31.7–35.9%, and 84.8–90.8%, respectively.

When the rotation angle was reduced from 360° to 180° , the reduction rates of the doses to the lenses, thyroid lobes, parotid glands, and sublingual glands were approximately 53.3–69.0%, 31.8–58.1%, 9.3–18.9%, and 20.1–45.0%, respectively.

Table 4 shows a comparison of this study with the study by Pauwels et al. [45]. The measured values cannot be directly compared because of the different measurement methods and imaging conditions. Therefore, the relative differences in radiation doses were compared. Pauwels et al. reported that the effect of FOVs and rotation angles on organ-absorbed doses in adult males. To measure the radiation dose for each exposure, thermoluminescent dosimeter (TLD) chips of the type TLD-100 (LiF:Mg,Ti) were used. Some of the dosimeters were inserted into the phantom. A tube voltage of 90 kV and tube current 5 mA were used. Lens, thyroid, and salivary gland doses were measured in the maxillary canine at the 4×4 cm FOV and in the maxillary midline at the 6×6 cm FOV. The salivary glands differed from this study because they were not divided into parotid, submandibular and sublingual glands. In addition, in this study, the number of measurements was three and the standard deviation (SD) was calculated, but in Pauwels' study, the number of measurements was not stated, and the SD was not calculated.

Table 2. The results of radiation doses to highly radiosensitive organs (mGy) measured with the maxillary median placed at the center of rotation.

| FOV (cm) | 4 × 4 | | | | 6 × 6 | | | |
|------------------------|--------------------------------|--------------------------------|-------------|--------------------------------|--------------------------------|--------------------------------|--------------------------------|--------------------------------|
| Rotation Angle (°) | 360 | | 180 | | 360 | | 180 | |
| Tube Current (mA) | 2 | 3 | 2 | 3 | 2 | 3 | 2 | 3 |
| Right lens | 0.08 ± 0.00 | 0.12 ± 0.00 | 0.03 ± 0.00 | 0.06 ± 0.00 | 0.20 ± 0.00 | 0.30 ± 4.96 × 10 ⁻³ | 0.07 ± 0.00 | 0.10 ± 0.00 |
| Left lens | 0.14 ± 0.00 | 0.19 ± 0.00 | 0.07 ± 0.00 | 0.09 ± 0.00 | 0.34 ± 4.80 × 10 ⁻³ | 0.46 ± 0.00 | 0.13 ± 4.80 × 10 ⁻³ | 0.18 ± 4.80 × 10 ⁻³ |
| Right lobe of thyroid | 0.22 ± 0.00 | 0.26 ± 0.00 | 0.12 ± 0.00 | 0.18 ± 0.00 | 0.61 ± 0.00 | 0.92 ± 0.00 | 0.30 ± 0.00 | 0.46 ± 0.00 |
| Left lobe of thyroid | 0.21 ± 0.00 | 0.32 ± 0.00 | 0.10 ± 0.00 | 0.14 ± 0.00 | 0.52 ± 9.04 × 10 ⁻³ | 0.78 ± 0.00 | 0.25 ± 0.00 | 0.37 ± 0.00 |
| Right parotid gland | 0.58 ± 4.96 × 10 ⁻³ | 0.84 ± 0.00 | 0.49 ± 0.00 | 0.75 ± 0.00 | 0.89 ± 0.00 | 1.31 ± 0.00 | 0.77 ± 4.96 × 10 ⁻³ | 1.13 ± 0.00 |
| Left parotid gland | 0.91 ± 4.80 × 10 ⁻³ | 1.30 ± 0.00 | 0.80 ± 0.00 | 1.16 ± 4.80 × 10 ⁻³ | 1.36 ± 4.80 × 10 ⁻³ | 1.95 ± 0.00 | 1.19 ± 0.00 | 1.72 ± 4.80 × 10 ⁻³ |
| Right sublingual gland | 0.22 ± 0.00 | 0.35 ± 4.94 × 10 ⁻³ | 0.13 ± 0.00 | 0.19 ± 4.94 × 10 ⁻³ | 1.58 ± 4.94 × 10 ⁻³ | 2.30 ± 0.00 | 1.14 ± 4.94 × 10 ⁻³ | 1.68 ± 4.94 × 10 ⁻³ |
| Left sublingual gland | 0.16 ± 0.00 | 0.27 ± 0.00 | 0.11 ± 0.00 | 0.17 ± 4.52 × 10 ⁻³ | 1.52 ± 4.52 × 10 ⁻³ | 2.26 ± 0.00 | 1.14 ± 0.00 | 1.70 ± 0.00 |

Data are presented as mean ± standard deviation.

Table 3. The results of radiation doses to highly radiosensitive organs (mGy) measured with the maxillary right canine tooth placed at the center of rotation.

| FOV (cm) | 4 × 4 | | | | 6 × 6 | | | |
|------------------------|--------------------------------|--------------------------------|--------------------------------|--------------------------------|--------------------------------|-------------|--------------------------------|--------------------------------|
| Rotation Angle (°) | 360 | | 180 | | 360 | | 180 | |
| Tube Current (mA) | 2 | 3 | 2 | 3 | 2 | 3 | 2 | 3 |
| Right lens | 0.10 ± 4.96 × 10 ⁻³ | 0.17 ± 0.00 | 0.03 ± 0.00 | 0.06 ± 4.96 × 10 ⁻³ | 0.25 ± 0.00 | 0.34 ± 0.00 | 0.08 ± 0.00 | 0.11 ± 0.00 |
| Left lens | 0.13 ± 0.00 | 0.19 ± 0.00 | 0.05 ± 4.80 × 10 ⁻³ | 0.08 ± 0.00 | 0.29 ± 4.80 × 10 ⁻³ | 0.39 ± 0.00 | 0.12 ± 4.80 × 10 ⁻³ | 0.16 ± 4.80 × 10 ⁻³ |
| Right lobe of thyroid | 0.17 ± 9.87 × 10 ⁻³ | 0.30 ± 0.00 | 0.07 ± 0.00 | 0.14 ± 0.00 | 0.53 ± 0.00 | 0.78 ± 0.00 | 0.24 ± 4.94 × 10 ⁻³ | 0.38 ± 4.94 × 10 ⁻³ |
| Left lobe of thyroid | 0.17 ± 1.20 × 10 ⁻³ | 0.29 ± 0.00 | 0.08 ± 4.52 × 10 ⁻³ | 0.14 ± 0.00 | 0.49 ± 0.00 | 0.74 ± 0.00 | 0.24 ± 0.00 | 0.37 ± 0.00 |
| Right parotid gland | 0.66 ± 4.96 × 10 ⁻³ | 0.98 ± 4.96 × 10 ⁻³ | 0.57 ± 4.96 × 10 ⁻³ | 0.84 ± 4.96 × 10 ⁻³ | 1.02 ± 0.00 | 1.50 ± 0.00 | 0.83 ± 4.96 × 10 ⁻³ | 1.23 ± 0.00 |
| Left parotid gland | 0.89 ± 4.80 × 10 ⁻³ | 1.28 ± 4.80 × 10 ⁻³ | 0.80 ± 4.80 × 10 ⁻³ | 1.16 ± 0.00 | 1.33 ± 4.80 × 10 ⁻³ | 1.91 ± 0.00 | 1.17 ± 4.80 × 10 ⁻³ | 1.70 ± 4.80 × 10 ⁻³ |
| Right sublingual gland | 0.25 ± 0.00 | 0.41 ± 0.00 | 0.16 ± 0.00 | 0.25 ± 0.00 | 1.94 ± 4.94 × 10 ⁻³ | 2.84 ± 0.00 | 1.31 ± 0.00 | 1.91 ± 4.94 × 10 ⁻³ |
| Left sublingual gland | 0.18 ± 0.00 | 0.27 ± 0.00 | 0.12 ± 0.00 | 0.19 ± 4.52 × 10 ⁻³ | 1.39 ± 4.52 × 10 ⁻³ | 2.02 ± 0.00 | 1.10 ± 0.00 | 1.62 ± 4.52 × 10 ⁻³ |

Data are presented as mean ± standard deviation.

Table 4. Radiation doses to highly radiosensitive organs (μGy) in this study compared to the study by Pauwels et al. [45].

| Position | This Study | | | | Pauwels et al. [45] | | | |
|--------------------|------------------|--------------|------------------|--------------|---------------------|-----|------------------|------|
| | Maxillary canine | | Maxillary median | | Maxillary canine | | Maxillary median | |
| Tube voltage (kV) | 90 | | 90 | | 90 | | 90 | |
| Tube current (mA) | 3 | | 3 | | 5 | | 5 | |
| FOV (cm) | 4 × 4 | | 6 × 6 | | 4 × 4 | | 6 × 6 | |
| Rotation angle (°) | 360 | 180 | 360 | 180 | 360 | 180 | 360 | 180 |
| Exposure time (s) | 17.5 | 9.0 | 17.5 | 9.0 | 17.5 | 9.0 | 17.5 | 9.0 |
| Lens | 38.3 ± 0.00 | 14.1 ± 0.50 | 72.7 ± 0.49 | 26.1 ± 0.48 | 174 | 95 | 608 | 288 |
| Thyroid | 51.1 ± 0.49 | 25.0 ± 0.00 | 147.4 ± 0.95 | 72.4 ± 0.00 | 108 | 50 | 175 | 88 |
| Parotid gland | 225.4 ± 0.98 | 199.5 ± 0.50 | 326.3 ± 0.50 | 284.3 ± 0.48 | - | - | - | - |
| Sublingual gland | 67.7 ± 0.00 | 43.7 ± 0.45 | 456.7 ± 2.26 | 338.0 ± 0.00 | - | - | - | - |
| Salivary gland | - | - | - | - | 845 | 573 | 2192 | 1583 |

Data in this study are presented as mean ± standard deviation.

4. Discussion

This study examined the effects of FOVs and rotation angles on radiation doses to highly radiosensitive organs in children undergoing dental CBCT.

Based on the results of this study, radiation doses to highly radiosensitive organs differed greatly depending on the FOV and rotation angle. It is self-evident that reducing the FOV and rotation angle reduces the radiation dose. However, as the rate of dose reduction varies among organs, it is important to consider the relative positions of different organs with respect to the FOV and the trajectory of the X-ray tube. Although this study measured surface doses rather than organ doses, it provides additional information that may be useful in reducing exposure dose in dental CBCT examinations. Based on the results of this study, the following conclusions were drawn.

The positional relationship between FOVs and RTDs is shown in Figure 5. The parotid gland doses were significantly higher than the other organ doses examined in the 4×4 cm FOV. Because the parotid glands are located at approximately the same height as the maxillary incisors and canines, the parotid glands were partially or fully irradiated by the primary X-ray beam. Compared with the 4×4 cm FOV, the sublingual gland doses increased significantly at the 6×6 cm FOV. This was because the primary X-ray beam irradiated the sublingual glands little or not at all in the 4×4 cm FOV and either partially or fully in the 6×6 cm FOV. The FOV should be as small as possible because sublingual gland doses can be significantly reduced by reducing the FOV from 6×6 cm to 4×4 cm. Since the lens and thyroid doses were small, lens and thyroid were not likely irradiated by the primary X-ray beam at both the 4×4 cm and 6×6 cm FOV. Therefore, the lens and thyroid doses were reduced from the 6×6 cm FOV to the 4×4 cm FOV because the scattered radiation doses decreased.

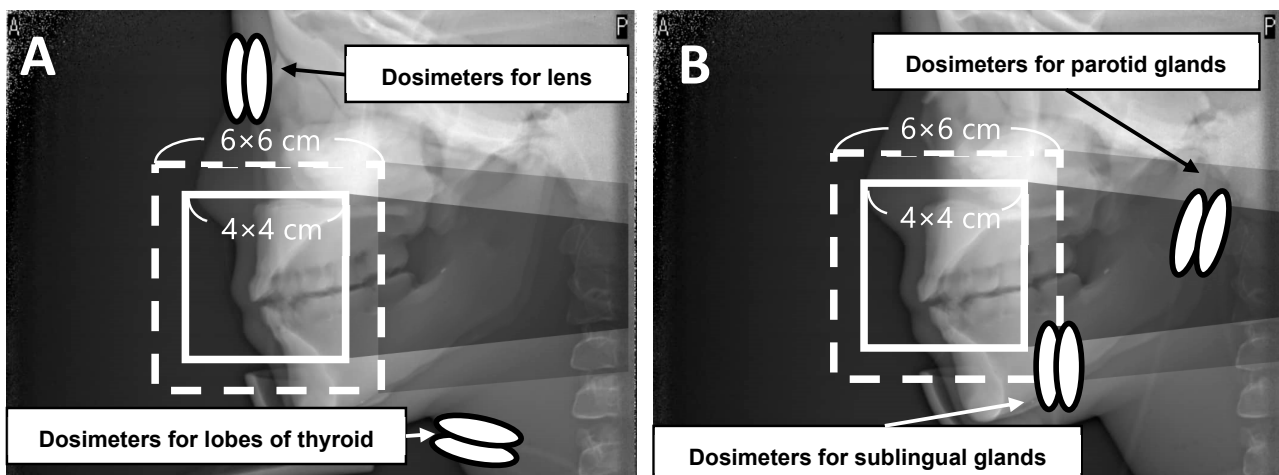


Figure 5. The positional relationship between FOVs and RTDs for (A) lenses and thyroid lobes and (B) parotid glands and sublingual glands.

All measured lens doses were significantly lower than the eye dose threshold for cataract induction, so children undergoing dental CBCT examinations to diagnose ectopic eruptions and impacted teeth are at a very low risk of developing cataracts.

The lens dose decreased the most among the organs examined when the rotation angle was reduced from 360° to 180° . This is related to the positions of the X-ray tube and lenses. At a 180° rotation, the X-ray tube rotated around the posterior aspect of the phantom. The lenses were placed in front of the head. Therefore, the lenses were irradiated by a reduced X-ray beam passing through the head and neck, which explains the reduced lens doses. The parotid glands are located on the side of the head and behind the center of rotation of the X-ray tube. Therefore, some of the X-ray beams directly irradiated the parotid glands without passing through the head; thus, the reduction rates in the parotid gland doses were the lowest. The dose reduction rates of the 180° rotation relative to the 360° rotation were

highest for the lens, followed by the thyroid, sublingual gland, and parotid gland, similar to the study by Vogiatzi et al. [67] using a large FOV (17×12 cm FOV).

Compared to the maxillary median, when the maxillary right canine was placed at the center of rotation, there was little difference in each dose at a 4×4 cm FOV. However, at a 6×6 cm FOV, the right sublingual gland dose was slightly higher. The right sublingual gland was included in the 6×6 cm FOV, which may have increased the effect of the primary X-ray beam. Careful consideration of the relative positions of the FOV and its organs is necessary, particularly when the FOV is large.

Pauwels et al. [45] reported the effects of FOVs and rotation angles on organ-absorbed doses in adult males. Compared to 6×6 cm FOV and the midline, 4×4 cm FOV and canine teeth showed greatly reduced lens doses in adults, whereas thyroid doses were greatly reduced in children. The difference in the scattered radiation dose due to differences in head and neck size between adults and children may have influenced the reduction rate. The reduction rates of the dose by decreasing the rotation angle were higher for the lenses and thyroid lobes than for the salivary glands, and similar results were obtained for both adults and children. As mentioned above, this is thought to be related to the location of the X-ray tube, lenses, thyroid lobes, and salivary glands. The reduction rates by FOV and rotation angle were different owing to different methods and phantom sizes but were all high, indicating that reducing the FOV and rotation angle was also useful in children.

Theodorakou et al. [37] reported the average organ-absorbed doses with various CBCT devices using a 10-year-old phantom. The results of the study by Theodorakou et al. were similar to those of this study, such that salivary glands irradiated by primary radiation received significantly higher doses than other organs. In a previous study by Theodorakou et al., the average salivary gland dose was >2.5 mGy and the average thyroid doses was 0.6 mGy. The average radiation doses to highly radiosensitive organs with optimal conditions (90 kV, 2 mA, 4×4 cm FOV, 180° rotation) in this study were 0.67 mGy for parotid glands, 0.13 mGy for sublingual glands, and 0.09 mGy for thyroid lobes, which were much lower than those reported by the study by Theodorakou et al. Theodorakou et al. used higher tube currents, larger FOVs, and 360° rotation. Special pediatric imaging conditions were not used in some of the devices, and the same imaging conditions for adults were used, which may have resulted in the radiation doses to highly radiosensitive organs. The target area included the maxillofacial and alveolar bones in addition to the teeth. A direct comparison of the doses for each imaging condition was not possible because the radiation doses to highly radiosensitive organs at the FOVs (4×4 and 6×6 cm) and rotation angles (360° and 180°) used in this study were not compared.

In our previous study [50], we investigated the optimal imaging conditions suitable for CBCT examinations for the diagnosis of ectopic eruption and impacted teeth in children, based on radiation doses and subjective and objective image quality evaluations. The optimal imaging conditions were 90 kV, 2 mA, 4×4 cm FOV, and 180° rotation. It was shown that reducing the tube current from 3 to 2 mA, the FOV from 6×6 to 4×4 cm, and the rotation angle from 360° to 180° resulted in poorer image quality due to image noise; however, the image quality was acceptable for diagnosis. However, clinical studies are needed in the future because the experiment was conducted using a phantom. Compared with the maximum imaging conditions (90 kV, 3 mA, 6×6 cm FOV, 360° rotation), the reduction rates of doses using the optimal conditions were 87.9% for lenses, 88.4% for thyroids, 60.1% for parotid glands, and 94.6% for sublingual glands. In this study, by measuring the radiation doses to highly radiosensitive organs, we substantiated the usefulness of reducing tube currents, FOVs, and rotation angles.

5. Conclusions

This study aimed to examine the effects of FOVs and rotation angles on radiation doses to highly radiosensitive organs in children using dental CBCT. By reducing the FOV from 6×6 cm to 4×4 cm, the dose to the sublingual gland could be decreased significantly. Additionally, by reducing the rotation angle from 360° to 180° , the lens dose

can be decreased significantly. Since the rate of dose reduction varies among organs, it is important to consider the relative positions of different organs with respect to the FOV and the trajectory of the X-ray tube. These results could help the formulation of low-dose protocols for the use of small FOVs for dental CBCTs in children.

Author Contributions: Conceptualization, K.C.; methodology, K.C.; software, M.I. (Misaki Ito); validation, M.I. (Misaki Ito) and K.C.; formal analysis, M.I. (Misaki Ito); investigation, M.I. (Misaki Ito), T.K. and M.F.; resources, M.I. (Masahiro Iikubo) and K.C.; data curation, M.I. (Misaki Ito), T.K. and M.F.; writing—original draft preparation, M.I. (Misaki Ito), M.S., I.K., S.O. and K.C.; writing—review and editing, M.I. (Misaki Ito), I.K., M.I. (Masahiro Iikubo), S.O., M.N., M.Z. and K.C.; visualization, M.I. (Misaki Ito); supervision, M.I. (Masahiro Iikubo) and K.C.; project administration, M.S., M.N., M.Z. and K.C.; funding acquisition, M.Z. and K.C. All authors have read and agreed to the published version of the manuscript.

Funding: This study was supported in part by a Grant-in-Aid for Scientific Research (20K10109) from the Japan Society for the Promotion of Science.

Institutional Review Board Statement: Not applicable.

Informed Consent Statement: Not applicable.

Data Availability Statement: Data are contained within the article.

Conflicts of Interest: The authors declare no conflicts of interest.

References

1. ICRP. Education and Training in Radiological Protection for Diagnostic and Interventional Procedures. ICRP Publication 113. *Ann. ICRP* **2009**, *39*, 7–68.
2. Chida, K. What are useful methods to reduce occupational radiation exposure among radiological medical workers, especially for interventional radiology personnel? *Radiol. Phys. Technol.* **2022**, *15*, 101–115. [[CrossRef](#)] [[PubMed](#)]
3. Chida, K.; Saito, H.; Otani, H.; Kohzuki, M.; Takahashi, S.; Yamada, S.; Shirato, K.; Zuguchi, M. Relationship between fluoroscopic time, dose—Area product, body weight, and maximum radiation skin dose in cardiac interventional procedures. *Am. J. Roentgenol.* **2006**, *186*, 774–778. [[CrossRef](#)] [[PubMed](#)]
4. ICRP. Radiological Protection in Medicine. ICRP Publication 105. *Ann. ICRP* **2007**, *37*, 1–63. Available online: <https://www.icrp.org/publication.asp?id=ICRP%20Publication%20105> (accessed on 26 August 2024).
5. ICRP. ICRP Statement on Tissue Reactions/Early and Late Effects of Radiation in Normal Tissues and Organs—Threshold Doses for Tissue Reactions in a Radiation Protection Context. ICRP Publication 118. *Ann. ICRP* **2012**, *41*, 1–322. Available online: <https://www.icrp.org/publication.asp?id=ICRP%20Publication%20118> (accessed on 26 August 2024). [[CrossRef](#)]
6. International Commission on Radiological Protection (ICRP). Statement on Tissue Reactions. Available online: <https://www.icrp.org/page.asp?id=123> (accessed on 26 August 2024).
7. IAEA TECDOC No.1731 Implications for Occupational Radiation Protection of the New Dose Limit for the Lens of the Eye; TECDOC Series. 2013. Available online: https://wwwpub.iaea.org/mtcd/publications/pdf/te-1731_web.pdf (accessed on 26 August 2024).
8. Chida, K.; Kaga, Y.; Haga, Y.; Kataoka, N.; Kumasaka, E.; Meguro, T.; Zuguchi, M. Occupational dose in interventional radiology procedures. *Am. J. Roentgenol.* **2013**, *200*, 138–141. [[CrossRef](#)]
9. Haga, Y.; Chida, K.; Kaga, Y.; Sota, M.; Meguro, T.; Zuguchi, M. Occupational eye dose in interventional cardiology procedures. *Sci. Rep.* **2017**, *7*, 569. [[CrossRef](#)]
10. Kato, M.; Chida, K.; Ishida, T.; Toyoshima, H.; Yoshida, Y.; Yoshioka, S.; Moroi, J.; Kinoshita, T. Occupational radiation exposure of the eye in neurovascular interventional physician. *Radiat. Prot. Dosim.* **2019**, *185*, 151–156. [[CrossRef](#)]
11. Endo, M.; Haga, Y.; Sota, M.; Tanaka, A.; Otomo, K.; Murabayashi, Y.; Abe, M.; Kaga, Y.; Inaba, Y.; Suzuki, M.; et al. Evaluation of novel X-ray protective eyewear in reducing the eye dose to interventional radiology physicians. *J. Radiat. Res.* **2021**, *62*, 414–419. [[CrossRef](#)]
12. Matsuzaki, S.; Moritake, T.; Morota, K.; Nagamoto, K.; Nakagami, K.; Kuriyama, T.; Kunugita, N. Development and assessment of an educational application for the proper use of ceiling-suspended radiation shielding screens in angiography rooms using augmented reality technology. *Eur. J. Radiol.* **2021**, *143*, 109925. [[CrossRef](#)]
13. Fujibuchi, T. Radiation protection education using virtual reality for the visualisation of scattered distributions during radiological examinations. *J. Radiol. Prot.* **2021**, *41*, S317–S328. [[CrossRef](#)] [[PubMed](#)]
14. Matsubara, K.; Takei, Y.; Mori, H.; Kobayashi, I.; Noto, K.; Igarashi, T.; Suzuki, S.; Akahane, K. A multicenter study of radiation doses to the eye lenses of medical staff performing non-vascular imaging and interventional radiology procedures in Japan. *Phys. Med.* **2020**, *74*, 83–91. [[CrossRef](#)] [[PubMed](#)]
15. Lang, N.P.; Hill, R.W. Radiographs in periodontics. *J. Clin. Periodontol.* **1977**, *4*, 16–28. [[CrossRef](#)] [[PubMed](#)]

16. Corbet, E.F.; Ho, D.K.L.; Lai, S.M.L. Radiographs in periodontal disease diagnosis and management. *Aust. Dent. J.* **2009**, *54*, S27–S43. [CrossRef] [PubMed]
17. Erdelyi, R.A.; Duma, V.F.; Sinescu, C.; Dobre, G.M.; Bradu, A.; Podoleanu, A. Dental Diagnosis and Treatment Assessments: Between X-rays Radiography and Optical Coherence Tomography. *Materials* **2020**, *13*, 4825. [CrossRef]
18. Preshaw, P.M. Detection and diagnosis of periodontal conditions amenable to prevention. *BMC Oral Health* **2015**, *15*, S5. [CrossRef]
19. Otaka, Y.; Harata, Y.; Izawa, M.; Iwawaki, A.; Ishii, T.; Saka, H.; Kito, S. Reduction of operator exposure by rectangular collimation in portable intraoral radiography. *Radiol. Phys. Technol.* **2020**, *13*, 312–320. [CrossRef]
20. Suomalainen, A.; Kiljunen, T.; Kaser, Y.; Peltola, J.; Kortensniemi, M. Dosimetry and image quality of four dental cone beam computed tomography scanners compared with multislice computed tomography scanners. *Dentomaxillofac. Radiol.* **2009**, *38*, 367–378. [CrossRef]
21. Loubele, M.; Bogaerts, R.; Van Dijck, E.; Pauwels, R.; Vanheusden, S.; Suetens, P.; Marchal, G.; Sanderink, G.; Jacobs, R. Comparison between effective radiation dose of CBCT and MSCT scanners for dentomaxillofacial applications. *Eur. J. Radiol.* **2009**, *71*, 461–468. [CrossRef]
22. Li, Y.; Huang, B.; Cao, J.; Fang, T.; Liu, G.; Li, X.; Wu, J. Estimating radiation dose to major organs in dental x-ray examinations: A phantom study. *Radiat. Prot. Dosim.* **2020**, *192*, 328–334. [CrossRef]
23. Shin, H.S.; Nam, K.C.; Park, H.; Choi, H.U.; Kim, H.Y.; Park, C.S. Effective doses from panoramic radiography and CBCT (cone beam CT) using dose area product (DAP) in dentistry. *Dentomaxillofac. Radiol.* **2014**, *43*, 20130439. [CrossRef]
24. Deman, P.; Atwal, P.; Duzenli, C.; Thakur, Y.; Ford, N.L. Dose measurements for dental cone-beam CT: A comparison with MSCT and panoramic imaging. *Phys. Med. Biol.* **2014**, *59*, 3201–3222. [CrossRef] [PubMed]
25. Smita, S.B.; Sara, A.; Basim, A.; Abdullah, A.; Abdullah, A.; Atul, B.; Ayoub, A. CBCT in Pediatric Dentistry: Awareness and Knowledge of Its Correct Use in Saudi Arabia. *Appl. Sci.* **2022**, *12*, 335. [CrossRef]
26. David, A.; Iga, S.; Bartusik-Aebisher, D. Temporary Skeletal Anchorage Devices and Cone Beam Tomography in Orthodontics—Current Application and New Directions of Development. *Appl. Sci.* **2024**, *14*, 5028. [CrossRef]
27. ICRP. Radiological Protection in Cone Beam Computed Tomography (CBCT). ICRP Publication 129. *Ann. ICRP* **2015**, *44*, 9–127. Available online: <https://www.icrp.org/publication.asp?id=ICRP%20Publication%20129> (accessed on 26 August 2024).
28. Hidalgo-Rivas, J.A.; Theodorakou, C.; Carmichael, F.; Murray, B.; Payne, M.; Horner, K. Use of cone beam CT in children and young people in three United Kingdom dental hospitals. *Int. J. Paediatr. Dent.* **2014**, *24*, 336–348. [CrossRef]
29. Ebru, A.; Büşra, K.E. Reasons for requesting cone-beam computed tomography in children and adolescents: A 10-year. *Biotechnol. Biotechnol. Equip.* **2022**, *36*, 858–864. [CrossRef]
30. Pearce, M.S.; Salotti, J.A.; Little, M.P.; McHugh, K.; Lee, C.; Kim, K.P.; Howe, N.L.; Ronckers, C.M.; Rajaraman, P.; Sir Craft, A.W.; et al. Radiation exposure from CT scans in childhood and subsequent risk of leukaemia and brain tumours: A retrospective cohort study. *Lancet* **2012**, *380*, 499–505. [CrossRef]
31. Mathews, J.D.; Forsythe, A.V.; Brady, Z.; Butler, M.W.; Goergen, S.K.; Byrnes, G.B.; Giles, G.G.; Wallace, A.B.; Anderson, P.R.; Guiver, T.A.; et al. Cancer risk in 680,000 people exposed to computed tomography scans in childhood or adolescence: Data linkage study of 11 million Australians. *BMJ* **2013**, *346*, f2360. [CrossRef]
32. Brenner, D.; Elliston, C.; Hall, E.; Berdon, W. Estimated risks of radiation-induced fatal cancer from pediatric CT. *Am. J. Roentgenol.* **2001**, *176*, 289–296. [CrossRef]
33. Higuchi, K.; Fujimura, T. Radiation exposure dose outside the irradiation field due to differences in pediatric head computed tomography scanning methods. *Radiol. Phys. Technol.* **2021**, *14*, 173–178. [CrossRef] [PubMed]
34. Nemoto, M.; Chida, K. Reducing the Breast Cancer Risk and Radiation Dose of Radiography for Scoliosis in Children: A Phantom Study. *Diagnostics* **2020**, *10*, 753. [CrossRef] [PubMed]
35. Chida, K.; Ohno, T.; Kakizaki, S.; Takegawa, M.; Yuuki, H.; Nakada, M.; Takahashi, S.; Zuguchi, M. Radiation dose to the pediatric cardiac catheterization and intervention patient. *Am. J. Roentgenol.* **2010**, *195*, 1175–1179. [CrossRef] [PubMed]
36. ICRP. Radiological Protection in Paediatric Diagnostic and Interventional Radiology. ICRP Publication 121. *Ann. ICRP* **2013**, *42*, 1–63. Available online: <https://www.icrp.org/publication.asp?id=ICRP%20Publication%20121> (accessed on 26 August 2024).
37. Theodorakou, C.; Walker, A.; Horner, K.; Pauwels, R.; Bogaerts, R.; Jacobs, R. Estimation of paediatric organ and effective doses from dental cone beam CT using anthropomorphic phantoms. *Br. J. Radiol.* **2012**, *85*, 153–160. [CrossRef]
38. Pauwels, R.; Cockmartin, L.; Ivanauskaitė, D.; Urbonienė, A.; Gavala, S.; Donta, C.; Tsiklakis, K.; Jacobs, R.; Bosmans, H.; Bogaerts, R.; et al. Estimating cancer risk from dental cone-beam CT exposures based on skin dosimetry. *Phys. Med. Biol.* **2014**, *59*, 3877–3891. [CrossRef]
39. Gallichan, N.; Albadri, S.; Dixon, C.; Jorgenson, K. Trends in CBCT current practice within three UK paediatric dental de-partments. *Eur. Arch. Paediatr. Dent.* **2020**, *21*, 537–542. [CrossRef]
40. Yiğit, T.; Yüksel, H.T.; Evirgen, Ş.; Kaçmaz, I.; Türkmenoğlu, A. Evaluation of use of cone beam computed tomography in paediatric patients: A cross-sectional study. *Int. J. Paediatr. Dent.* **2023**, *33*, 468–476. [CrossRef]
41. Rallan, M.; Rallan, N.S.; Goswami, M.; Rawat, K. Surgical management of multiple supernumerary teeth and an impacted maxillary permanent central incisor. *BMJ Case Rep.* **2013**, *2013*, bcr2013009995. [CrossRef]
42. Sharma, A.; Singh, V.P. Supernumerary Teeth in Indian Children: A Survey of 300 Cases. *Int. J. Dent.* **2012**, *2012*, 745265. [CrossRef]

43. Rajab, L.D.; Hamdan, M.A. Supernumerary Teeth in Indian Children: A Survey of 300 Cases. *Int. J. Paediatr. Dent.* **2002**, *12*, 244–254. [[CrossRef](#)] [[PubMed](#)]
44. SEDENTEXCT Radiation Protection no 172. Cone Beam CT for Dental and Maxillofacial Radiology. Evidence-Based Guidelines. Luxembourg: European Commission. Available online: [https://www.orthodont-cz.cz/data/files/sedentext\(1\).pdf](https://www.orthodont-cz.cz/data/files/sedentext(1).pdf) (accessed on 7 April 2023).
45. Pauwels, R.; Zhang, G.; Theodorakou, C.; Walker, A.; Bosmans, H.; Jacobs, R.; Bogaerts, R.; Horner, K. Effective radiation dose and eye lens dose in dental cone beam CT: Effect of field of view and angle of rotation. *Br. J. Radiol.* **2014**, *87*, 20130654. [[CrossRef](#)] [[PubMed](#)]
46. Hirsch, E.; Wolf, U.; Heinicke, F.; Silva, M.A. Dosimetry of the cone beam computed tomography Veraviewepocs 3D compared with the 3D Accuitomo in different fields of view. *Dentomaxillofac Radiol.* **2008**, *37*, 268–273. [[CrossRef](#)] [[PubMed](#)]
47. Grüning, M.; Koivisto, J.; Mah, J.; Bumann, A. Impact of thyroid gland shielding on radiation doses in dental cone beam computed tomography with small and medium fields of view. *Oral Surg. Oral Med. Oral Pathol. Oral Radiol.* **2022**, *134*, 245–253. [[CrossRef](#)]
48. Hajem, S.; Brogårdh-Roth, S.; Nilsson, M.; Hellén-Halme, K. CBCT of Swedish children and adolescents at an oral and maxillofacial radiology department. A survey of requests and indications. *Acta Odontol. Scand.* **2020**, *78*, 38–44. [[CrossRef](#)]
49. Ito, M.; Onodera, S.; Kojima, I.; Chida, K. Effect of different rotation angle on image quality in dental CBCT: Physical evaluation. *Medical Imaging and Information Sciences (MII)* **2022**, *39*, 38–42. (In Japanese) [[CrossRef](#)]
50. Ito, M.; Chida, K.; Onodera, S.; Kojima, I.; Iikubo, M.; Kato, T.; Fujisawa, M.; Zuguchi, M. Evaluation of radiation dose and image quality for dental cone-beam computed tomography in pediatric patients. *J. Radiol. Prot.* **2023**, *43*, 031518. [[CrossRef](#)]
51. UK Guidance National Diagnostic Reference Levels (NDRs) from 13 October 2022, Updated 24 November 2022. Available online: www.gov.uk/government/publications/diagnostic-radiology-national-diagnostic-reference-levels-ndr/ndr (accessed on 28 March 2023).
52. Seehra, J.; Yaqoob, O.; Patel, S.; O’Neill, J.; Bryant, C.; Noar, J.; Morris, D.; Cobourne, M.T. National clinical guidelines for the management of unerupted maxillary incisors in children. *Br. Dent. J.* **2018**, *224*, 779–785. [[CrossRef](#)]
53. Suresh, K.S.; Uma, H.L.; Nagarathna, J.; Kumar, P. Management of Ectopically Erupting Maxillary Incisors: A Case Series. *Int. J. Clin. Pediatr. Dent.* **2015**, *8*, 227–233. [[CrossRef](#)]
54. Anthonappa, R.P.; Omer, R.S.; King, N.M. Characteristics of 283 supernumerary teeth in southern Chinese children. *Oral Surg. Oral Med. Oral Pathol. Oral Radiol. Endod.* **2008**, *105*, e48–e54. [[CrossRef](#)]
55. Seehra, J.; DiBiase, A.T.; Patel, S.; Stephens, R.; Littlewood, S.J.; Spencer, R.J.; Frawley, T.; Benson, P.E.; Ireland, A.J.; Parvizi, F.; et al. Study protocol for the management of impacted maxillary central incisors: A multicentre randomised clinical trial: The iMAC Trial. *Trials* **2022**, *23*, 787. [[CrossRef](#)] [[PubMed](#)]
56. Noda, T.; Takagi, M.; Hayashi-Sakai, S.; Taguchi, Y. Eruption disturbances in Japanese children and adolescents. *Pediatr. Dent. J.* **2006**, *16*, 50–56. [[CrossRef](#)]
57. Einy, S.; Michaeli-Geller, G.; Aizenbud, D. Eruption Treatment of Impacted Teeth Following Surgical Obstruction Removal. *Appl. Sci.* **2022**, *12*, 449. [[CrossRef](#)]
58. Nagaraj, K.; Upadhyay, M.; Yadav, S. Impacted maxillary central incisor, canine, and second molar with 2 supernumerary teeth and an odontoma. *Am. J. Orthod. Dentofac. Orthop.* **2009**, *135*, 390–399. [[CrossRef](#)] [[PubMed](#)]
59. Ericson, S.; Kuroi, J. Longitudinal study and analysis of clinical supervision of maxillary canine eruption. *Community Dent. Oral. Epidemiol.* **1986**, *14*, 172–176. [[CrossRef](#)] [[PubMed](#)]
60. Ahmed, M.A.; Zaki, H. Root Resorption of Adjacent Teeth Associated with Maxillary Canine Impaction in the Saudi Arabian Population: A Cross-Sectional Cone-Beam Computed Tomography Study. *Appl. Sci.* **2022**, *12*, 334. [[CrossRef](#)]
61. Nikhil, P.; Seema, D.B.; Swara, H.S.; Bhavna, H.D. Supplementary Tooth: To Extract or Observe? Evidence Based Practice with the Literature Review. *Adv. Hum. Biol.* **2015**, *5*, 92–101. [[CrossRef](#)]
62. Inaba, Y.; Nakamura, M.; Zuguchi, M.; Chida, K. Development of novel real-time radiation systems using 4-channel sensors. *Sensors* **2020**, *20*, 2741. [[CrossRef](#)]
63. Kato, M.; Chida, K.; Nakamura, M.; Toyoshima, H.; Terata, K.; Abe, Y. New real-time patient radiation dosimeter for use in radiofrequency catheter ablation. *J. Radiat. Res.* **2019**, *60*, 215–220. [[CrossRef](#)]
64. Nakamura, M.; Chida, K.; Zuguchi, M. Red emission phosphor for real-time skin dosimeter for fluoroscopy and interventional radiology. *Med. Phys.* **2014**, *41*, 101913. [[CrossRef](#)]
65. Fontana, R.C.; Pasqual, E.; Miller, D.L.; Simon, S.L.; Cardis, E.; Thierry-Chef, I. Trends in Estimated Thyroid, Salivary Gland, Brain, and Eye Lens Doses From Intraoral Dental Radiography Over Seven Decades (1940 TO 2009). *Health Phys.* **2020**, *118*, 136–148. [[CrossRef](#)] [[PubMed](#)]
66. International Commission on Radiation Units and Measurements. *Tissue Substitutes in Radiation Dosimetry and Measurement*; ICRU: Bethesda, MD, USA, 1989.
67. Vogiatzi, T.; Menz, R.; Verna, C.; Bornstein, M.M.; Dagassan-Berndt, D. Effect of field of view (FOV) positioning and shielding on radiation dose in paediatric CBCT. *Dentomaxillofac. Radiol.* **2022**, *51*, 20210316. [[CrossRef](#)] [[PubMed](#)]

Disclaimer/Publisher’s Note: The statements, opinions and data contained in all publications are solely those of the individual author(s) and contributor(s) and not of MDPI and/or the editor(s). MDPI and/or the editor(s) disclaim responsibility for any injury to people or property resulting from any ideas, methods, instructions or products referred to in the content.